Journal of Power Sources 196 (2011) 8340–8345

Contents lists available at ScienceDirect

Journal of Power Sources

journal homepage: www.elsevier.com/locate/jpowsour

Changes in electronic states of platinum–cobalt alloy catalyst for polymer electrolyte fuel cells by potential cycling

Shoichi Hidai[a,b,*], Masaki Kobayashi[a,c], Hideharu Niwa[a], Yoshihisa Harada[a,c], Masaharu Oshima[a,c], Yoji Nakamori[b], Tsutomu Aoki[b]

[a] Department of Applied Chemistry, School of Engineering, The University of Tokyo, Hongo, Bunkyo-ku, Tokyo 113-8656, Japan
[b] Toshiba Fuel Cell Power Systems Corporation, Ukishima-cho, Kawasaki-ku, Kawasaki-shi, Kanagawa 210-0862, Japan
[c] Synchrotron Radiation Research Organization, The University of Tokyo, Hongo, Bunkyo-ku, Tokyo 113-8656, Japan

ARTICLE INFO

Article history:
Received 29 March 2011
Received in revised form 20 May 2011
Accepted 15 June 2011
Available online 22 June 2011

Keywords:
PEFC
Cathode catalyst
Pt–Co alloy
Durability
X-ray photoemission spectroscopy

ABSTRACT

Changes in the electronic states of platinum–cobalt (Pt–Co) alloy catalysts through potential cycling between 0.6 and 1.0 V were investigated by X-ray photoemission spectroscopy (XPS) using synchrotron radiation. The electrochemical surface area loss and the particle size growth of the Pt catalyst were larger than those of the Pt–Co alloy catalyst. Pt 4*f* XPS spectra of the Pt–Co alloy catalyst do not show any change through the potential cycling, indicating that most part of Pt is stable during the potential cycling. Larger amount of $Pt(OH)_2$ existed in the initial MEA of the Pt catalyst than the Pt–Co alloy catalyst, indicating that the Pt catalyst has a tendency to be oxidized. The $Pt(OH)_2$ decreased and metallic platinum increased in the cycle-tested MEA, suggesting that the $Pt(OH)_2$ dissolved and re-deposited as metallic states. The oxidation tendency explains the less durability of the Pt catalyst than the Pt–Co alloy catalyst. Co 2*p* XPS spectra imply that cobalt is absent on the surface of the catalyst particles and the Pt skin layer is thicker than 1.4 nm (4 mono-layers). The absence of the cobalt oxide in the cycle-tested MEA demonstrates that the Pt–Co core under the Pt skin layer is stable during the potential cycling.

1. Introduction

Polymer electrolyte fuel cell (PEFC) systems have been developed as next generation power sources for stationary, portable or transport applications. As a PEFC generates electricity, heat, and water through the electrochemical reactions, the PEFC system can operate at high efficiency, with low levels of noise and CO_2 emission. These features make the PEFC system an environmentally friendly power source. However, the cost and durability are still recognized as the primary issues for the commercialization [1]. In order to enhance the rate of electrochemical reactions, platinum nano-particles loaded on carbon support are widely employed as cathode catalyst in PEFCs [1]. As platinum is rare metal and is expensive, minimizing the level of platinum loading is effective in reducing the cost of the PEFC systems. On decreasing the platinum loading, both high electrochemical activity and high durability are required to maintain the PEFC performance. Pt–M alloy (M: 3*d* transition metal) is one of the most promising candidate materials to decrease platinum loading for PEFC cathodes because of its high oxygen reduction reaction activity which is greater than that of a platinum catalyst [2–4]. Among the Pt–M alloy catalysts, the Pt–Co alloy catalyst shows the highest activity [2–4]. The electronic states of platinum in Pt–M alloy catalysts are believed to play an important role on the high catalytic activity. A lot of works have been reported recently based on the relation between the catalytic activity and the position of the *d*-band center [2–6].

In order to improve the performance of Pt–M alloy catalysts, however, it is necessary to understand not only the origin of the high catalytic activity but also the degradation mechanism in Pt–M alloy catalysts in comparison with the Pt catalyst. It is reported that the degradation of the Pt nano-particle catalysts for PEFCs is caused by the growth of Pt nano-particles, which is so called Ostwald ripening [7–10]. The Pt dissolution and the deposition on the other particles are the mechanism of Ostwald ripening. Part of the dissolved Pt move toward an electrolyte membrane and deposit inside and/or interface of the membrane [10]. Mitsushima et al. [11] show the Pt dissolution follows the Pt oxidation. Zhang et al. [12] measured the electronic states of Pt 4*f* using X-ray photoelectron spectroscopy (XPS) and found that the amount of the Pt oxide was increased after the PEFC operation for 200 h.

* Corresponding author. Tel.: +81 44 288 8021; fax: +81 44 288 8212.
E-mail addresses: shoichi.hidai@toshiba.co.jp, hidai@sr.t.u-tokyo.ac.jp (S. Hidai).

0378-7753/$ – see front matter © 2011 Elsevier B.V. All rights reserved.
doi:10.1016/j.jpowsour.2011.06.054

The durability of the Pt–Co alloy catalyst has also been studied by many groups. Yu et al. [13] have confirmed that the Pt–Co alloy catalyst is more durable and shows less cell-performance decay than the Pt catalyst after the exposure to potential cycling between 0.87 and 1.23 V. It is also reported that the Pt–Co alloy catalyst can prevent the particle growth and the loss of active electrochemical surface area (ECA) compared to the platinum catalyst [14,15]. However, it is pointed out that cobalt is easily dissolved out of the catalyst particle from the beginning of the operation [13,14,16]. The cobalt dissolution might cause a serious problem from the viewpoint of the durability because it decreases the mass activity down to the level as low as the conventional Pt catalyst. In order to investigate the relationship between the degradation of Pt–Co alloy catalysts and their surface oxidation behavior, we have analyzed the Pt–Co alloy catalyst in PEFC stack operated for 6700 h in an internal humidification system. We revealed by soft X-ray absorption spectroscopy that less than 10% of Co was oxidized, while the cell performance was degraded by 3% [17]. In our Pt–Co alloy catalysts, less Co dissolution was observed than that reported in previous studies. Chen et al. [18] suggest that the Pt-enriched surface layer is produced by acid treatment and improves the durability of the Pt–Co alloy catalyst.

In the present study, we aimed to evaluate the high durability of the Pt–Co alloy catalysts in comparison with the conventional Pt catalyst. We have investigated the change in the oxygen reduction reaction activities of Pt–Co alloy catalysts used in membrane electrode assembly (MEA) during potential cycling test which accelerates the catalyst degradation. The electronic states of cobalt and platinum have been evaluated by X-ray photoemission spectroscopy (XPS) using synchrotron radiation in order to correlate them with the Pt–Co alloy catalyst degradation. To obtain the in-depth information on chemical bonding states in the catalyst particles, hard X-rays and soft X-rays having larger and shorter probing depths were used for the XPS measurements. The changes in the electronic states of platinum during PEFC operation are expected to directly reflect the change in the reactivity of platinum. By comparing the XPS results with the electrochemical measurement results, the degradation mechanism of the Pt–Co alloy catalyst in the MEA is discussed.

2. Experiments

The Pt–Co alloy catalyst used in this study was TEC36E52 (made by Tanaka Kikinzoku Kogyo). Atomic ratio of platinum to cobalt was about 3:1 in the alloy, and the platinum concentration was 47 wt%. As the Pt catalyst TEC10E50E (made by Tanaka Kikinzoku Kogyo) was used. Their nano-particles were loaded on Ketjen black with 47 wt% platinum to make a catalyst powder. The catalyst powder was mixed with an ionomer solution to produce a catalyst ink which was spread on a support film as a decal sheet. A pair of the decal sheets was hot-pressed on an electrolyte membrane to construct an MEA. A pair of non-woven carbon sheets covered with a micro porous layer was attached on both sides of the MEA as gas diffusion layers (GDLs).

Potential cycling was applied to accelerate catalyst degradation. The cell temperature was maintained at 80 °C by external heaters. Fully humidified hydrogen was introduced to the anode and fully humidified nitrogen to the cathode. Square-shaped potential waves were applied to the cell by 10,000 cycles. The potential was kept at 0.6 V for 3 s and 1.0 V for another 3 s in one cycle. The potential condition was selected to minimize the carbon corrosion which might be significant over 1.0 V [19,20]. The drained water from the cell was condensed and the amount of dissolved platinum and cobalt in the water were measured by atomic absorption spectrophotometry (AAnalyst 600, Perkin Elmer).

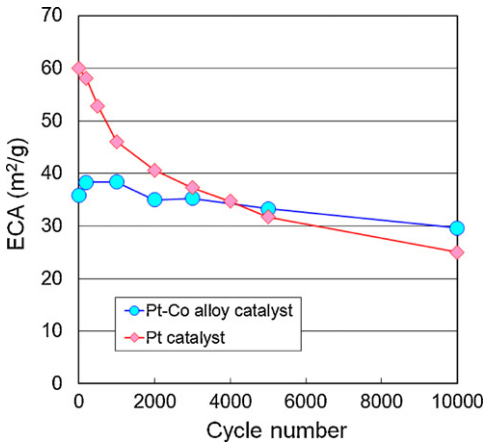

Fig. 1. Electrochemical surface area (ECA) changes of Pt–Co alloy catalyst and Pt catalyst in the potential cycling test. Circle symbols are Pt–Co alloy catalyst and triangle symbols are Pt catalyst.

The catalyst performance was evaluated by ECA measurements. ECA was calculated by integrating hydrogen adsorption charge in cyclic voltammogram (CV) measurements and dividing it by 0.21 mC cm^{-2}. The CV measurements were conducted at cell temperature of 30 °C. Fully humidified hydrogen was introduced to the anode, while fully humidified nitrogen was introduced to the cathode. The potential was applied from 0.05 V to 1.0 V with a sweep rate of 10 mV s^{-1}, regulated using an electrochemical measurement system (HZ5000, Hokuto Denko).

Transmission electron microscopy (TEM) images were obtained to investigate the catalyst particle size and the structural change of the catalyst layer. Transmission electron microscope (H-7100FA, Hitachi) was operated at an acceleration voltage of 100 keV. The particle size of the cathode catalysts was evaluated from the TEM images.

Hard X-ray photoemission spectroscopy (HXPES) experiments were performed *ex situ* at the beam line BL47XU of SPring-8. The photon energy was set at about 8 keV, where the energy resolution was $E/\Delta E > 20{,}000$. The measurements were conducted in an ultra-high vacuum below 3×10^{-7} Pa at room temperature. The probing depth of the HXPES photoelectrons from Pt atoms was approximately 18 nm. Soft X-ray photoemission spectroscopy (SXPES) was conducted at the beam line BL27SU of SPring-8. The photon energy was set at 1 keV, where the energy resolution was $E/\Delta E \sim 5000$. The measurements were conducted in an ultra-high vacuum below 4×10^{-8} Pa at room temperature. The probing depth of the SXPES photoelectrons was approximately 3.4 nm. The XPS measurements were conducted on the catalyst powder, initial MEA and cycle-tested MEA. For MEA samples, GDLs were removed and X-rays were irradiated on the GDL side of the cathode catalyst layer.

3. Results and discussion

3.1. Electrochemical and micro structure changes

Fig. 1 shows the ECA loss of the Pt–Co alloy catalyst during potential cycling compared with the Pt catalyst. The ECA of the Pt–Co alloy catalyst decreased from 36 m^2 g^{-1} to 30 m^2 g^{-1} through the potential cycling, corresponding to 17% loss of the ECA. The initial ECA of the Pt catalyst was larger than that in the Pt–Co catalyst because of the smaller size of the particles. However, the ECA loss of the Pt catalyst was 58% and was much larger than that of the Pt–Co alloy catalyst, resulting in almost the same ECA of the Pt catalyst as that of the Pt–Co alloy catalyst after 10,000 times of potential cycling.

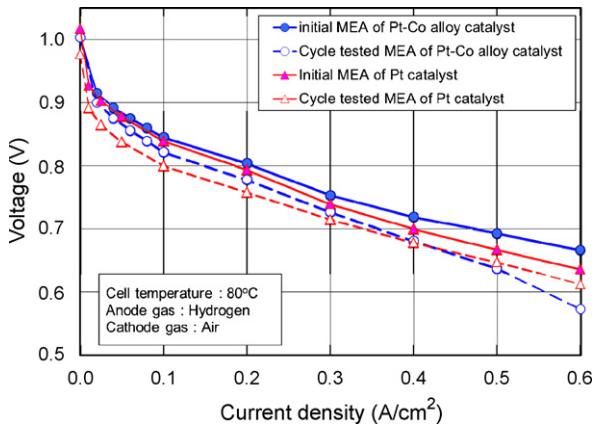

Fig. 2. Load calibration curves comparison between Pt–Co alloy catalyst and Pt catalyst for the initial MEAs and the cycle-tested MEAs. Circle symbols are Pt–Co alloy catalyst and triangle symbols are Pt catalyst. Solid lines show the performance of the initial MEA and the dash lines show the performance of the cycle-tested MEA. The cell temperature is 80 °C and the fully humidified hydrogen is introduced to anode and 66% RH air to cathode.

The changes in the cell performance from the initial MEA to the cycle-tested MEA are compared between the Pt–Co alloy catalysts and the Pt catalyst in Fig. 2. The cell voltage drop for the Pt catalyst in the low current density region, which is caused by the catalytic activity loss, is much larger than that for the Pt–Co alloy catalyst. The active over potential of the Pt catalyst at 0.3 A cm^{-2} decreased by 38 mV, while that of the Pt–Co alloy catalyst decreased by 21 mV. These results are consistent with the difference in the ECA loss between two catalysts. The cell voltage of the Pt–Co alloy catalyst also decreases in the higher current density region than 0.5 A cm^{-2}. This is originated not from the catalytic activity loss but from increase in the diffusion over potential. Small portion of hydrophilic functional group might be produced on the surface of the carbon support even under 1.0 V and might make the catalyst layer hydrophilic. Therefore product water on the carbon support might prevent the gas diffusion [21].

Fig. 3 shows histograms of the particle sizes of initial MEAs and cycle-tested MEAs measured from the TEM images. The distribution of the particle size for the Pt–Co alloy catalyst in the cycle-tested MEA is similar to that for the initial MEA, as shown in Fig. 3(a). The mean values of the particle size for the initial and the cycle-tested MEAs are 6.1 nm and 5.9 nm, respectively, indicating that the Ostwald ripening mechanism cannot apply to the Pt–Co alloy catalyst and thus explaining why the catalytic activity loss is very small at the low current region in Fig. 2. As for the Pt catalyst, the average particle size increased from 2.5 nm to 5.7 nm, and the peak widths were broadened, as shown in Fig. 3(b). As has been reported, the particle growth in this case is caused by the Ostwald ripening process [7–10].

We have confirmed by the atomic absorption spectrophotometry that platinum did not dissolve into water drain from the tested cell for both catalysts, which suggests that all platinum atoms remain in the MEA. Part of platinum dissolved from the catalyst may migrate and deposit in the electrolyte membrane. The ECA decay of the Pt catalyst might include the effect of the deposits in the electrolyte membrane besides the particle size growth. Therefore the ECA decay of Pt–Co alloy catalyst shown in Fig. 1 was caused by the deposits in the electrolyte membrane. Yu et al. [13] reported that the deposits of Pt catalyst after potential cycling is larger than Pt–Co alloy catalyst in electrolyte membrane. As a result, the ECA of the Pt catalyst after 10,000 cycles is smaller than that of Pt–Co alloy catalyst even the particle size was smaller than the Pt–Co alloy catalyst.

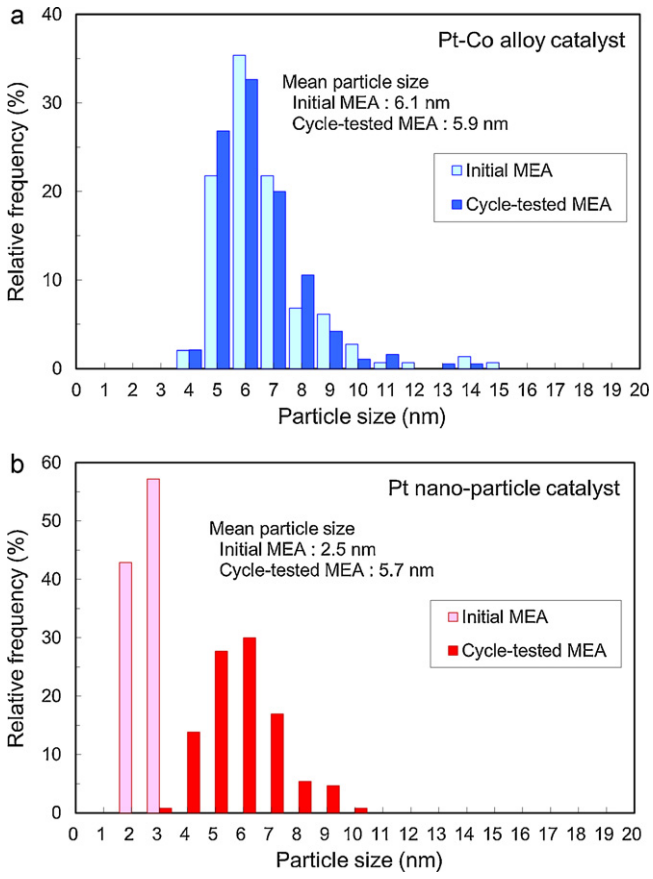

Fig. 3. Histogram of the particle sizes measured using the TEM images for (a) Pt–Co catalyst and (b) Pt catalyst. The light color bars represent the histogram of the initial MEA and the dark color bars represent that of the cycle-tested MEA.

3.2. XPS measurements of Pt 4f

Pt 4*f* SXPES and HXPES spectra of Pt–Co alloy catalysts under various conditions (catalyst powder, initial MEA and cycle-tested MEA) are shown in Fig. 4. SXPES and HXPES provide surface and full area information of the Pt–Co nano-particle since the probing depth of SXPES (3.4 nm) and HXPES (18 nm) are smaller and larger, respectively, than the average particle size of the Pt–Co alloy catalysts (~6 nm). Because the SXPES and HXPES results showed almost the same profile, only the SXPES results are discussed hereafter. Vertical lines represent the Pt $4f_{7/2}$ and $4f_{5/2}$ peak positions of a Pt foil as a reference. All the Pt 4*f* spectra show energy shifts toward higher binding energy from the reference. The energy shift of 0.3 eV for the Pt–Co catalyst powder can be mostly explained by the chemical shift partly due to Pt–Co alloy formation, which has been already reported by Mun et al. [5].

In order to investigate the Pt–Co alloying effect on Pt chemical states, we have compared the chemical states of the Pt–Co alloy with those of the Pt catalyst under various conditions (catalyst powder, initial MEA and cycle-tested MEA). Since the probing depth of SXPES (3.4 nm) is larger than the average particle size of the Pt catalyst (2.5 nm) of the initial MEA and is smaller than the average particle size of the Pt catalyst (5.7 nm) of the cycle-tested MEA, the SXPES spectra of the Pt catalyst provides bulk information for initial MEA and surface information for cycle-tested MEA. The Pt 4*f* SXPES spectra of the Pt catalyst are compared with those of the Pt–Co alloy catalysts in Fig. 5. The catalyst powder and the initial MEA of the Pt catalyst show broader peaks than those for the Pt–Co alloy catalyst, suggesting that platinum oxides exist on the Pt catalyst. Thus the Pt catalyst can be easily oxidized in the atmosphere.

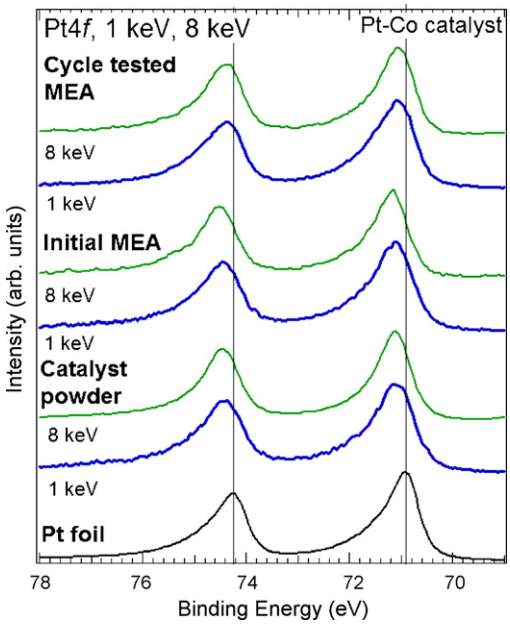

Fig. 4. X-ray photoemission spectra of Pt 4*f* core level for catalyst powder, initial MEA, cycle-tested MEA and Pt foil as a reference. Thin lines represent HXPES (8 keV) spectra and bold lines represent SXPES (1 keV) spectra. Vertical lines shows the positions of metallic Pt 4*f* peaks obtained from Pt foil measurement.

On the other hand, the cycle-tested MEA of the Pt catalyst seems to contain mainly metallic platinum probably because Pt re-deposited on the Pt catalyst surface by the Ostwald ripening process exists as the metallic state.

The relative contents of the Pt chemical states obtained from the peak fitting of the Pt 4*f* SXPES results are shown in Fig. 6. The spectra are decomposed into the metallic state, Pt^0, oxygen adsorbed platinum, PtO_{ads}, platinum hydroxide, $Pt(OH)_2$, and platinum oxides, PtO and PtO_2. The shift energies of those chemical components from the metallic state are listed in Table 1. The chemical states of the

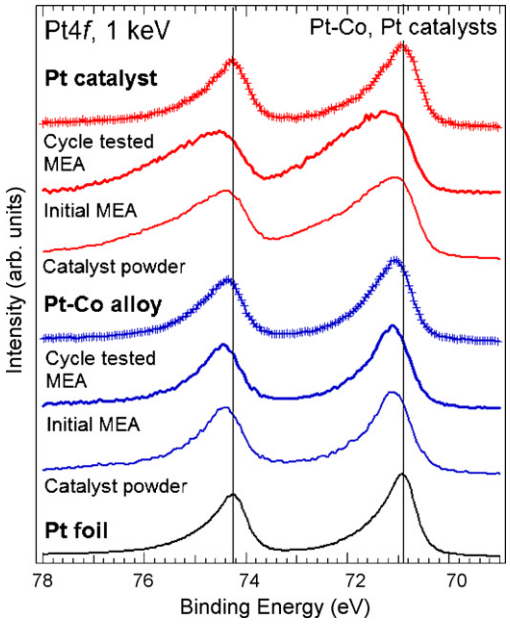

Fig. 5. SXPES spectra comparison between Pt–Co alloy catalyst and Pt catalyst. Upper three lines, are the spectra of Pt catalyst, middle three lines, are those of Pt–Co alloy catalyst and the lowest line is that of Pt foil as a reference. Thin lines are catalyst powder, thick lines are initial MEA and lines with symbols are cycle tested MEA.

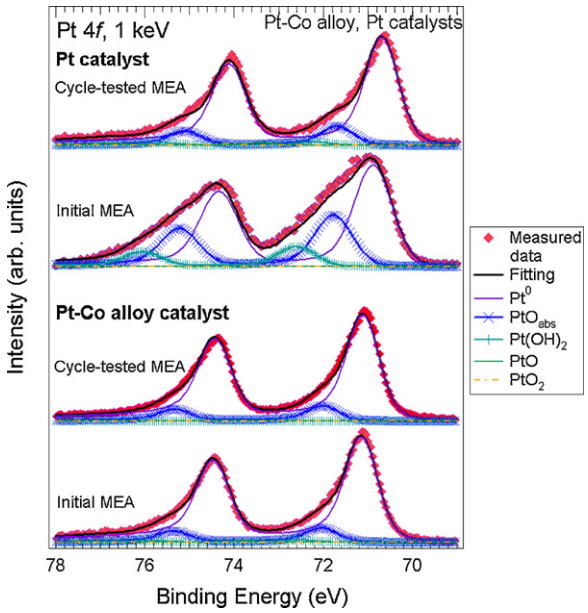

Fig. 6. Peak fitting of Pt 4*f* spectrum measured with 1 keV SXPES for Pt–Co alloy and Pt catalyst.

Pt–Co alloy catalysts are almost the same both in the initial MEA and the cycle-tested MEA, suggesting that most of Pt was stable during the potential cycling. Small portion of platinum hydroxide in the initial MEA might dissolve and disappeared in the cycle-tested MEA. On the other hand, the Pt catalyst contains more platinum hydroxide than the Pt–Co alloy catalyst. The oxygen adsorbed platinum in the Pt catalyst possibly decreased with the decrease of the surface region by the particle growth.

The Pt–Co alloy catalyst has less oxygen adsorbed platinum and platinum hydroxide than the Pt catalyst both in the initial MEA and the cycle-tested MEA. Pt–Co alloying should have an effect to reduce the surface oxidation. The Pt chemical shift might reduce the bonding energy between surface platinum and oxygen and prevent the platinum dissolution from the surface of the catalyst. On the other hand, the large particle size might be one of the causes to prevent the surface oxidization and decrease the ECA decay of the Pt–Co alloy catalyst. It is difficult to separate the particle size effect from the composition or alloy effect on Pt–Co alloy catalyst, as the particle size must increase by annealing in alloying process. From the surface component analysis, the surface oxidization seems to be a key factor for platinum dissolution. As the *d*-band center shift of Pt–Co alloy weakens the binding energy between surface platinum and adsorbed oxygen, the alloying should have an effect to prevent the surface oxidization and platinum dissolution. These results are consistent with the small decrease of the ECA in the Pt–Co alloy catalyst. On the contrary, most of the platinum hydroxide in the initial MEA of Pt catalyst dissolves during the potential cycling and is re-deposited in the metallic state for the cycle tested MEA.

3.3. XPS measurements of Co 2p

Co 2*p* HXPES spectra of the catalyst powder, the initial MEA and the cycle-tested MEA of the Pt–Co alloy catalyst are exhibited in Fig. 7. The profiles and the peak positions of the spectra are similar to that of metallic cobalt, suggesting that the cobalt atoms in the Pt–Co cathode catalysts exist mostly in a metallic phase. If a cobalt atom could detach from a catalyst particle, the detached cobalt atom is easily oxidized under the acidic condition during electrochemical operation and therefore exist as a cobalt oxide. However, a cobalt oxide peak expected at 780 eV [17,22] did not appear in

Table 1
Peak position and concentration of Pt chemical states obtained from peak fitting.

Sample	Pt $4f_{7/2}$ peak position (eV)	Concentration of Pt chemical states (%)					
		Chemical states Energy shift from Pt^0 (eV)	Pt^0 0	PtO_{ads} 0.9 [23]	$Pt(OH)_2$ 1.4 [24]	PtO 2.6 [23]	PtO_2 4.4 [23]
Pt–Co alloy catalyst Initial MEA	71.1		86	12	2	1	0
Pt–Co alloy catalyst Cycle-tested MEA	71.1		87	13	0	0	0
Pt catalyst Initial MEA	70.8		59	30	12	0	0
Pt catalyst Cycle-tested MEA	70.7		80	14	2	2	1

the cycle-tested MEA. This implies that cobalt in the Pt–Co alloy is stable against the potential cycling. Another result that explains the stability of cobalt in the Pt–Co alloy is shown by Co 2*p* SXPES in Fig. 7. Almost no signal of Co can be seen for all the samples. Since the probing depth of the Co atoms in the Pt–Co alloy catalyst is 1.4 nm, the absence of Co signal in the SXPES measurements suggests that cobalt resides in the bulk region deeper than 1.4 nm from the top surface of nano-particles, which corresponds to 4 mono-layers as the Pt atomic diameter is 0.3 nm. It has been reported that the annealed Pt–Co alloy catalysts have a platinum-rich skin layer on the surface called "Pt skin layer" [3]. The absence of cobalt on the surface verifies the presence of the Pt skin layer. Toda et al. [2] reported the calculated thickness of the Pt skin layer to be about 1 nm. Although model analyses are reported assuming the Pt skin layer thickness of one mono-layer [3,25,26], our result suggests that the highly dispersed Pt–Co nano-particles have Pt skin layers thicker than 4 mono-layers. As the particle size of the Pt–Co alloy catalyst widely distributed from 4 nm to 15 nm as shown in Fig. 3(a), the size of the core alloy should distribute from 1 nm to 12 nm. As a result, the ratio of Co over Pt might be smaller than average in the small size particle as they only have small alloy core.

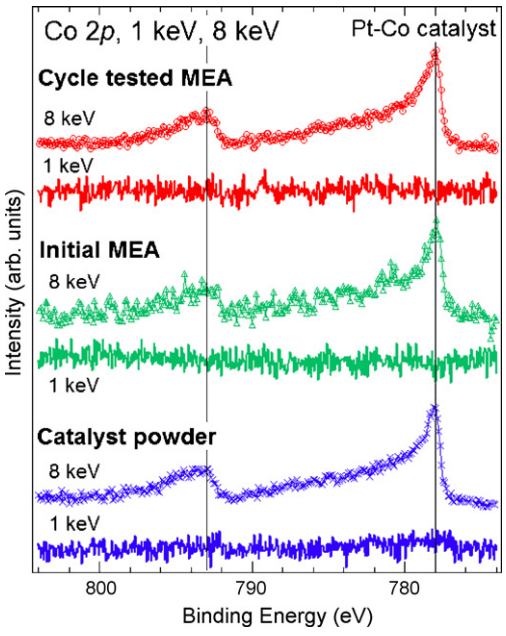

Fig. 7. X-ray photoemission spectra of Co 2*p* core level for catalyst powder, initial MEA, cycle-tested MEA. Thin lines with markers represent HXPES (8 keV) spectra and bold lines represent SXPES (1 keV) spectra. Vertical lines shows the positions of metallic Co 2*p* peaks.

As the cobalt peak did not appear even in the cycle-tested MEA, the Pt skin layer still exists after the potential cycling and prevents the formation of the cobalt oxide at the surface of the catalyst particles. The Pt skin layer can effectively protect the Pt–Co alloy in the core part of the catalyst from dissolution. Thick Pt skin layer might significantly improve the Pt–Co alloy catalyst durability.

4. Conclusions

We have evaluated the durability of Pt–Co alloy catalysts applied in MEA during potential cycling between 0.6 and 1.0 V. The Pt–Co alloy catalyst showed less ECA decay, particle growth and cell performance decay than Pt catalyst, suggesting higher durability than Pt catalyst. The chemical state of Pt measured by XPS showed less $Pt(OH)_2$ exists in the Pt–Co alloy catalyst than the Pt catalyst and suggests that the Pt–Co alloy catalyst is robust against oxidization in the atmosphere. By the potential cycling, the platinum hydroxide decreased and metallic platinum increased in the Pt catalyst, suggesting that platinum hydroxide dissolved and platinum was re-deposited in metallic states. The chemical state of the Pt–Co alloy catalyst did not show significant change even after potential cycling. It means that the surface Pt on the Pt–Co alloy catalyst is more stable than Pt catalyst. The Co 2*p* SXPES spectra of the Pt–Co catalyst revealed the absence of cobalt in the surface region of the catalyst particles, which indicates the presence of the Pt skin layer on the catalyst surface. Estimated from the probing depth of SXPES measurements, the Pt skin layer is thicker than 1.4 nm, corresponding to more than 4 mono-layers. The absence of the cobalt oxide in the cycle-tested MEA suggests that the surface Pt skin layer protects the Pt–Co core during the potential cycling.

Acknowledgements

This work was supported by New Energy and Industrial Technology Development Organization (NEDO). The authors would like to thank Dr. Ikenaga and Dr. Muro for their technical supports on HXPES and SXPES measurements at SPring-8.

References

[1] H.A. Gasteiger, S.S. Kocha, B. Sompalli, F.T. Wagner, Appl. Catal. B: Environ. 56 (2005) 9–35.
[2] T. Toda, H. Igarashi, H. Uchida, M. Watanabe, J. Electrochem. Soc. 146 (1999) 3750–3756.
[3] V.R. Stamenkovic, B.S. Mun, M. Arenz, K.J.J. Mayrhofer, C.A. Lucas, G. Wang, P.N. Ross, N.M. Markovic, Nat. Mater. 6 (2007) 241–247.
[4] V. Stamenkovic, B.S. Mun, K.J.J. Mayrhofer, P.N. Ross, N.M. Markovic, J. Rossmeisl, J. Greeley, J.K. Norskov, Angew. Chem. Int. Ed. 45 (2006) 2897–2901.
[5] B.S. Mun, M. Watanabe, M. Rossi, V. Stamenkovic, N.M. Markovic, P.N. Ross Jr., J. Chem. Phys. 123 (2005) 204717.

[6] M. Wakisaka, H. Suzuki, S. Mitsui, H. Ushida, M. Watanabe, J. Phys. Chem. C 112 (2008) 2750–2755.
[7] M.S. Wilson, F.H. Garzon, K.E. Sickafus, S. Gottesfeld, J. Electrochem. Soc. 140 (1993) 2872–2877.
[8] P.J. Ferreira, G.J. Ia O', Y. Shao-Horn, D. Morgan, R. Makharia, S. Kocha, H.A. Gasteiger, J. Electrochem. Soc. 152 (2005) A2256–A2271.
[9] E. Guilminot, A. Corcella, M. Chatenet, F. Millard, F. Charlot, G. Berthome, C. Iojoiu, J.Y. Sanchez, E. Rossinot, E. Claude, J. Electrochem. Soc. 154 (2007) B1106–B1114.
[10] Y. Shao-Horn, W.C. Sheng, S. Chen, P.J. Ferreira, E.F. Holby, D. Morgan, Top. Catal. 46 (2007) 285–305.
[11] S. Mitsushima, S. Kawahara, K. Ota, N. Kamiya, J. Electrochem. Soc. 154 (2007) B153–B158.
[12] F.-Y. Zhang, S.G. Advani, A.K. Prasad, M.E. Boggs, S.P. Sullivan, T.P. Beebe Jr., Electrochim. Acta 54 (2009) 4025–4030.
[13] P. Yu, M. Pemberton, P. Plasse, J. Power Sources 144 (2005) 11–20.
[14] H.R. Colon-Mercado, B.N. Popov, J. Power Sources 155 (2006) 253–263.
[15] A. Stassi, E. Modica, V. Antonucci, A.S. Arico, Fuel Cells 9 (2009) 201–208.
[16] S.C. Zignani, E. Antolini, E.R. Gonzalez, J. Power Sources 182 (2008) 83–90.
[17] M. Kobayashi, S. Hidai, H. Niwa, Y. Harada, M. Oshima, Y. Horikawa, T. Tokushima, S. Shin, Y. Nakamori, T. Aoki, Phys. Chem. Chem. Phys. 11 (2009) 8226–8230.
[18] S. Chen, H.A. Gasteiger, K. Hayakawa, T. Tada, Y. Shao-Horn, J. Electrochem. Soc. 157 (2010) A82–A97.
[19] L.M. Roen, C.H. Paik, T.D. Jarvi, Electrochem. Solid-State Lett. A 19 (2004) A19–A22.
[20] T. Kinumoto, K. Takai, Y. Iriyama, T. Abe, M. Inaba, Z. Ogumi, J. Electrochem. Soc. 153 (2006) A58–A63.
[21] T. Aoki, A. Matsunaga, Y. Ogami, A. Maekawa, S. Mitsushima, K. Ota, H. Nishikawa, J. Power Sources 195 (8) (2010) 2182–2188.
[22] C.D. Wagner, W.M. Riggs, L.E. Davis, J.F. Moulder, G.E. Mullenberg, Handbook of X-ray Photoelectron Spectroscopy, Perkin-Elmer Corp., 1979.
[23] K.S. Kim, N. Winograd, R.E. Davis, J. Am. Chem. Soc. 93 (1971) 6296–6297.
[24] J.S. Hammond, N. Winograd, J. Electroanal. Chem. 78 (1977) 55–69.
[25] V.R. Stamenkovic, T.J. Schmidt, P.N. Ross, N.M. Markovic, J. Phys. Chem. B 106 (2002) 11970–11979.
[26] V.R. Stamenkovic, B. Fowler, B.S. Mun, G. Wang, P.N. Ross, C.A. Lucas, N.M. Markovic, Science 315 (2007) 493–497.